Plasmon excitations in graphitic carbon spheres measured by EELS

Thomas Stöckli,* Jean-Marc Bonard, and André Châtelain
Institut de Physique Expérimentale, Département de Physique, Ecole Polytechnique Fédérale de Lausanne, CH - 1015 Lausanne, Switzerland

Zhong Lin Wang
School of Materials Science and Engineering, Georgia Institute of Technology, Atlanta, Georgia 30332-0245

Pierre Stadelmann
Centre Interdépartemental de Microscopie Electronique, Ecole Polytechnique Fédérale de Lausanne, CH - 1015 Lausanne, Switzerland
(Received 11 June 1999)

The determination of the physical properties of individual nanometer-size particles has made rapid progress with the availability of local probe techniques during the past years. Electron energy-loss spectroscopy in a high-resolution transmission electron microscope is one experimental tool that can give insight into the intriguing properties of such small particles. The interpretation of the experimental data of the plasmon excitations is well established in the case of isotropic particles of different geometries. For the case of anisotropic particles such as multiwall fullerenes (carbon onions), the interpretation schemes had to be reviewed. In a recent publication, we have proposed a formalism based on nonrelativistic local dielectric response theory for high-energy transmission electron microscopy electrons penetrating or passing close by an anisotropic particle [Stöckli *et al.*, Phys. Rev. B **57**, 15599 (1998)]. Here we report a detailed comparison of experimental data with the excitation probabilities obtained within this formalism. We show that there is an excellent agreement between theory and experiment. In consequence, we are able to interpret the plasmon loss data of multiwall fullerenes and draw conclusions on their physical properties.

I. INTRODUCTION

Nested concentric-shell fullerenes[1] (carbon onions) consist of several graphene sheets rolled up into spheres. They are arranged concentrically in a way that the intershell distance is approximately equal to the interlayer spacing of turbostratic planar graphite.[1,2] Like single-wall fullerenes,[3,4] single-wall nanotubes,[5,6] and multiwall nanotubes,[7] nested concentric-shell fullerenes belong to the so-called carbon nanostructures. These molecular structures of pure carbon have a variety of intriguing properties different from the other allotropic forms of carbon, graphite and diamond.

The first clue that the physical properties of carbon nanostructures differ from those of diamond and graphite came from fullerene C_{60}. By means of molecular-beam experiments it has been established that these molecules are semiconducting.[8] When bulk production methods became available,[9] it was found that fullerite (crystalline form of C_{60}) is semiconducting when pure[10,11] and that it can even be superconducting when doped.[12] Upon the discovery of tubular structures[7] theoretical considerations hinted for more surprising properties. Single-wall carbon nanotubes were predicted to be either semimetallic or semiconducting depending on their geometry.[13–15] Furthermore, coiled tubules[16] are proposed to be candidates for superconducting nanowires.[17] Not only the electronic properties of carbon nanostructures are predicted to be particular. Simulations carried out for single-wall carbon nanotubes suggest that their magnetic[18,19] and elastic properties[20] are different from those of graphite and diamond.

Unlike the case of single-wall fullerenes, for which the experimental determination of the physical properties started with the development of bulk-size crystal production methods,[9] the characterization of the multiwall spherical and the single- and multiwall tubular structures is difficult. Even though important progress has been made recently, the purity required for a comparison of data obtained from bulk characterization techniques with simulations carried out for individual particles has not yet been obtained. The standard production[21–23] and purification methods[24,25] still yield a mixture of particles of different geometries.

Recently, experiments using local probe techniques such as field emission,[26] atomic force,[27] and scanning tunnelling microscopy[28–31] have been designed to determine the physical properties of individual particles. For tubular structures there is now a lot of data available, giving important information on their electronic properties and confirming theoretical predictions to a great extent. However, only little is known about the physical properties of multiwall spherical structures. In our approach, we have used a somewhat less popular local probe technique, electron energy-loss spectroscopy (EELS) in a high-resolution transmission electron microscope (HRTEM), to get some insight into the electronic properties of spherical structures. EELS in this configuration offers the same advantages as the techniques just mentioned: one single particle can be selected, its structure can be determined, and measurements can be carried out as a function of the position of the probe on the particle. Moreover, the nested concentric-shell fullerenes can be produced directly in the microscope[1] so that bulk production methods requiring a

different experimental setup[32,33] are not necessary.

Even though the synthesis and the EELS measurements can be carried out in one working step in an adequately equipped TEM, only one transmission EELS study on individual multiwall fullerenes has yet been reported.[34] The authors analyze the changes in the bonding between the carbon atoms as a multiwall fullerene is transformed into diamond when irradiated with 1.25-MeV electrons.[35] However, the excitation of plasmons is not addressed in detail. This is probably due to the fact that the interpretation of plasmon-loss EEL data of individual nanometer-size particles relies on the comparison with simulated spectra. Unfortunately, the standard interpretation framework of the energy loss of a TEM probe electron due to plasmon excitations of small particles (nonrelativistic local dielectric response theory[36]) cannot be used for the interpretation of the data of carbon nanoparticles. The formalism assumes the particles to be isotropic, which is clearly not the case for nested concentric-shell fullerenes. As for planar graphite, it must be assumed that the electronic properties in the directions parallel or perpendicular to the grapitic shells are different. For the case of TEM electrons passing close by an isolated spherical graphitic particle Lucas *et al.* have expanded the basic interpretation scheme to take into account this anisotropy.[37] This formalism has been used by Henrard *et al.* to interpret plasmon-loss spectra of a square millimeter size area of thin films of multiwall fullerenes[32] obtained by reflection EELS.[38]

In a recent publication[39] we have generalized the formalism for anisotropic particles to include the case of penetrating electrons. Now, we are able to report a detailed comparison of the simulated excitation probabilities with experimental data. Our measurements have been carried out on individual particles in transmission geometry and are therefore particularly well suited for a comparison with the model.

II. EXPERIMENTAL DETAILS

A. Specimen preparation

Nested concentric-shell fullerenes have been prepared *in situ* by intense electron irradiation of polyhedral graphitic particles[1] as obtained in the standard arc deposition method used for the production of carbon nanotubes.[3] A small quantity of the black powder contained in the deposit was ultrasonically dispersed in ethanol. For TEM observations a holey carbon grid was dipped into the resulting dispersion and then left to dry, leaving enough carbon particles for the experiments. In order to synthesize multiwall fullerenes, a couple of polyhedral particles of reasonable size were selected and the electron beam was focused onto the zone of interest. At the same time all limiting apertures were opened in order to maximize the electron flux. In one of the microscopes (Hitachi HF 2000) a heating specimen holder has been used in order to accelerate the formation process.[2]

B. Electron Microscopy

In this paper, we have used two techniques for the analysis of the energy loss of the TEM probe electrons. In the first, a very small region of the sample (<2 nm^2) is selected and the loss spectrum of the selected spot is recorded on a detector array after passage through the energy-dispersive magnetic prism. The spot of interest can be selected either by irradiation with a nanometer-size electron probe or by the use of a small spectrometer aperture at high magnification.[40] In the second experiment, a sophisticated electron optical system at the exit of the energy-dispersive device is used to form an image of the sample with electrons that have lost a given amount of energy.[40] In an ideal case, this allows the localization of the origin of a feature of the loss spectrum on the sample, for instance at an interface or in regions of different chemical compositions.[36,40] The measurements have been carried out at the Centre Interdéparemental de Microscopie Electronique at the Swiss Federal Institute of Technology in Lausanne, where two experimental setups are available: a Hitachi HF 2000 field emission microscope equipped with a Gatan parallel detection EEL spectrometer (model 666) and a Philips CM 300 Schottky emitter microscope with a Gatan Imaging Filter.

Due to the difference in design and, in consequence, performance of the two energy analyzers, energy filtered images and spectra contain complementary information. With the available instruments and in the particular case of our low-loss study the spectroscopic method gives better energy resolution while the energy filtered imaging method gives better spatial resolution. When small probes are used to acquire spectra of a selected zone, the spatial resolution is determined by the size of the electron probe. Under optimum conditions probes as small as 2-nm diameter can be produced with the Hitachi microscope. When the zone is selected by a limiting spectrometer entrance aperture, the spatial resolution is determined by the diameter of the aperture, chromatic aberrations, and the image magnification. In the plasmon region, where chromatic aberrations can be neglected,[41] the Hitachi can be operated in conditions, which produce a comparable spatial resolution: the smallest spectrometer aperture of 1 mm and a magnification of 700 000 times allow one to select areas as small as 1.7 nm^2. In the imaging technique, the spatial resolution is limited by the imperfections of the electron optics. In the plasmon region, we have been able to achieve atomic resolution on the carbon nanostructures. This means that under these operating conditions the point to point resolution is better than 0.36 nm. The energy resolution of our spectroscopy setup is given by the full width at half maximum of the zero-loss intensity, which is between 0.45 and 0.55 eV. In the imaging setup the energy resolution is determined by the chromatic aberrations of the optical system. For the Gatan energy filter mounted on the CM 300 the smallest possible energy window imposed by these aberrations is 4 eV.

C. Determination of the plasmon excitation probability from the experimental data

In order to compare the experimental data from EEL measurements (filtered images and spectra) with the simulations of the plasmon losses of multishell fullerenes, it is necessary to find the relation between the observed intensity and the excitation probability. The observed signal $J(\omega)$ is the superposition of the signal of the electrons that have passed through the sample without energy loss $J_0(\omega)$, the signal of the electrons that have undergone one collision $J_1(\omega)$, and

of the signal of the electrons that have interacted several times with the sample $J_2(\omega)$, $J_3(\omega)$ etc.

$$J(\omega)=J_0(\omega)+J_1(\omega)+J_2(\omega)+\cdots. \tag{1}$$

The integrated intensities I_n originating from the same number of collisions in the sample follow the Poisson distribution[40]

$$I_n=I^{\mathrm{tot}}\frac{1}{n!}\left(\frac{t}{\lambda}\right)^n\exp\left(-\frac{t}{\lambda}\right), \tag{2}$$

where I^{tot} is the total number of incident electrons, t is the thickness of the sample where the electron passes, and λ is the mean free path of the excitation. In an ideal experiment without any instrumental broadening the zero-loss intensity can be represented by a delta function

$$J_0(\omega)=I_0\delta(\omega)=I^{\mathrm{tot}}\exp\left(-\frac{t}{\lambda}\right)\delta(\omega). \tag{3}$$

The intensity of the electrons having undergone one single scattering event is proportional to the plasmon excitation probability $dP(\omega)/d\omega$ as obtained from the nonrelativistic local dielectric response theory (α constant):

$$J_1(\omega)=\alpha\frac{dP(\omega)}{d\omega}. \tag{4}$$

For the case of nested concentric-shell fullerenes and, in general, of any nanometer-size particle the excitation probability is composed of two contributions:

$$\frac{dP(\omega)}{d\omega}=\frac{dP^{\mathrm{surface}}(\omega)}{d\omega}+\frac{dP^{\mathrm{volume}}(\omega)}{d\omega}. \tag{5}$$

$dP^{\mathrm{surface}}(\omega)/d\omega$ is the surface plasmon excitation probability and $dP^{\mathrm{volume}}(\omega)/d\omega$ is the excitation probability of the volume plasmon. It is given for an electron passing at a given impact parameter through a particle of given size. When several components contribute to the total excitation probability the mean free path λ in the Poisson distribution can be replaced by the average mean free path λ_{av}:[42]

$$\frac{1}{\lambda_{\mathrm{av}}}=\frac{1}{\lambda_{\mathrm{surface}}}+\frac{1}{\lambda_{\mathrm{volume}}}, \tag{6}$$

where $1/\lambda_{\mathrm{surface}}$ and $1/\lambda_{\mathrm{volume}}$ are defined as

$$\frac{1}{\lambda_{\mathrm{surface}}}=\frac{1}{t}\int_0^\infty\frac{dP^{\mathrm{surface}}(\omega)}{d\omega}d\omega \tag{7a}$$

and

$$\frac{1}{\lambda_{\mathrm{volume}}}=\frac{1}{t}\int_0^\infty\frac{dP^{\mathrm{volume}}(\omega)}{d\omega}d\omega, \tag{7b}$$

respectively. Integrating the expression of $J_1(\omega)$ over the energy and using the Poisson distribution for the integrated intensities, the constant α is determined and $J_1(\omega)$ becomes

$$J_1(\omega)=I^{\mathrm{tot}}\frac{dP(\omega)}{d\omega}\exp\left(-\frac{t}{\lambda_{\mathrm{av}}}\right)=I_0\frac{dP(\omega)}{d\omega}. \tag{8}$$

The nested concentric-shell fullerenes investigated in this study are sufficiently small that it is reasonable to suppose that no multiple scattering occurs, so that all $J_n(\omega)$ with $n\geqslant 2$ become negligibly small and the observed signal is in a good approximation given by

$$J(\omega)=I_0\left[\delta(\omega)+\frac{dP(\omega)}{d\omega}\right]. \tag{9}$$

Equation (9) is the starting point for any direct comparison of EELS data to simulated excitation probabilities. After extraction of the zero-loss peak and division by the zero-loss intensity the experimental spectra acquired from a small region of the sphere can directly be compared to the simulated plasmon excitation probability at a given impact parameter. The energy filtered images acquired with a given energy window divided by the no-loss image give the excitation probability integrated over the energy window as a function of the impact parameter.

It has to be noticed that Eq. (9) has been established assuming ideal experimental conditions. TEM's are not ideal instruments in the sense that the incident electrons have a finite energy distribution and that the illuminating electron beam is not perfectly parallel. In consequence, the experimental absorption features will be broader than the peaks of the simulated excitation probabilities. Image acquisition can introduce further errors. In our experimental setups the electrons were detected via a scintillator on a slow scan charge coupled diode (CCD) camera. The conversion from the probe-electron to a photon in the scintillator and from the photon back to an electron in the CCD device is a statistical process. Two electrons incident on the same spot of the scintillator must not necessarily be detected by the same diode of the camera. Moreover, the detective quantum efficiency of the camera and noise introduced by its electronics can lead to differences between the actual number of incident electrons and the counts recorded on the CCD camera.[43]

For the comparison of our experimental data with the simulations we have taken into account the effects of the energy distribution of the incident electrons. All spectra have been deconvoluted with the experimentally determined energy distribution of the incident electrons (loss spectrum acquired without a specimen). The other factors affecting a direct comparison are experimentally hard to access and have not been taken into account.

III. EXPERIMENTAL DATA COMPARED TO SIMULATIONS

The discussion of the experimental data of multiwall fullerenes is divided into two parts. In the first part, the overall tendencies of intensity line profiles across energy filtered images and energy-loss spectra are compared with the simulated curves obtained from nonrelativistic local dielectric response theory[39] (Sec. III A). All excitation probabilities shown here have been simulated using the dielectric tensor determined by EELS measurements. The differences between the dielectric tensor determined by optical methods as compared to EELS and the resulting deviations in the simulations have been discussed in Ref. 39. In the second part a more detailed analysis of the important characteristics of the loss data is given (Sec. III B). Of particular interest is the

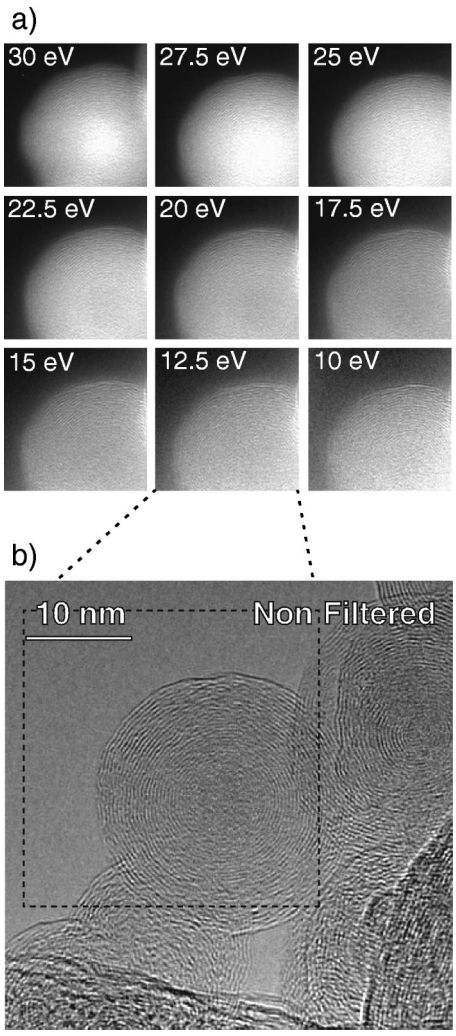

FIG. 1. (a) Series of energy filtered images of the nested concentric-shell fullerene shown in (b). The energy window was 4 eV, centered at the values indicated on the corresponding filtered image.

size dependence of these features, especially as the spheres become smaller. Section III C discusses the features of the experimental data that cannot be explained with our model.

A. General tendencies

Figure 1(a) displays a series of energy filtered images of the indicated region of the nested concentric-shell fullerene shown in Fig. 1(b). The sphere has a radius of 12.6 nm and was suspended over a hole in the holey carbon microscopy grid. The images in Fig. 1(a) have been taken with an 4 eV window centered at the indicated energies.

As discussed in Sec. II C, the filtered images have been divided by the image taken with the energy window centered on the zero-loss peak. In consequence, the gray levels are a direct measure of the plasmon excitation probability at a given position of the image integrated over the energy window. It can be observed that the intensity distribution changes as the window is shifted from 30 to 10 eV. At energies close to 27 eV the intensity is clearly maximal in the center of the sphere. At around 17 eV the intensity is distributed much more uniformly over the entire sphere.

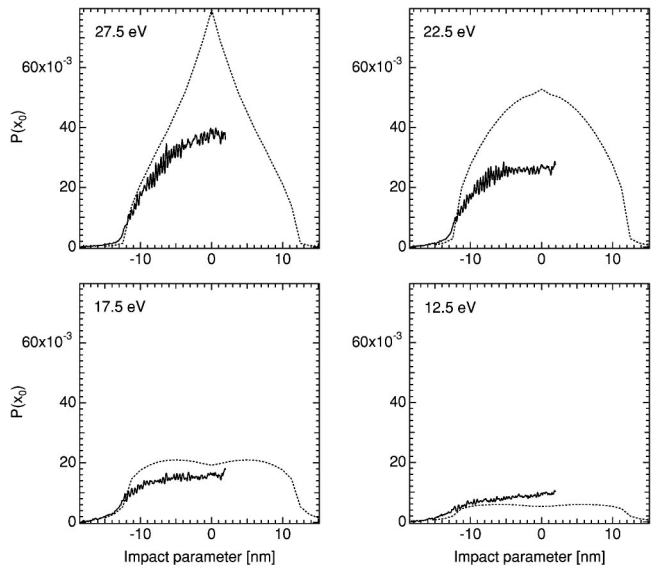

FIG. 2. Intensity line profiles for several selected energy windows of the filtered images displayed in Fig. 1. They are compared with the simulated line profiles obtained from non-relativistic local dielectric response theory (dotted line).

A quantitative comparison with the simulations can be accomplished when intensity line profiles across the energy filtered images are analyzed. Due to the rotational symmetry of the particles we have restrained the analysis to the portion between the center of the particle and the sphere boundary, a couple of nm into the vacuum.

Figure 2 shows intensity line profiles of four selected energy windows out of those shown in Fig. 1. They are compared to simulated profiles of an anisotropic sphere of 12.5 nm radius. Note that the scales in Fig. 2 are absolute and that the experimental data has not been adjusted to the simulated curves in any way. It can be seen that the dielectric treatment of the problem leads to the right order of magnitude of the excitation probability. Moreover, the simulated curves reproduce well the observed tendency, namely that the intensity distribution is peaked in the center of the sphere at 27.5 eV and that it becomes uniform over the entire sphere as the energy window is successively placed at lower energies. This is a clear piece of evidence in favor of the anisotropic formalism we have developed. In fact, the simulations[39] and the experimental data show that for this size of particle the corrections of the volume excitations due to the surface plasmons (Begrenzungseffect[44]) are rather weak. The shape of the intensity line profile of an isotropic sphere would therefore in good approximation be determined by the volume contribution of the total plasmon excitation probability. This in term would be proportional to the distance the electron travels in the medium, i.e., $P(x_0) \propto \sqrt{a^2 - x_0^2}$, with a the radius and x_0 the impact parameter. The behavior observed for multiwall fullerenes is clearly different and only the anisotropic formalism allows to explain it.

The intensity line profiles in Fig. 2 furthermore contain evidence for the presence of surface excitations. This becomes apparent when the region close to the interface sphere-vacuum is investigated in more detail (Fig. 3). It can be seen that the excitation probability just outside the sphere does not immediately drop to zero. This can only by ex-

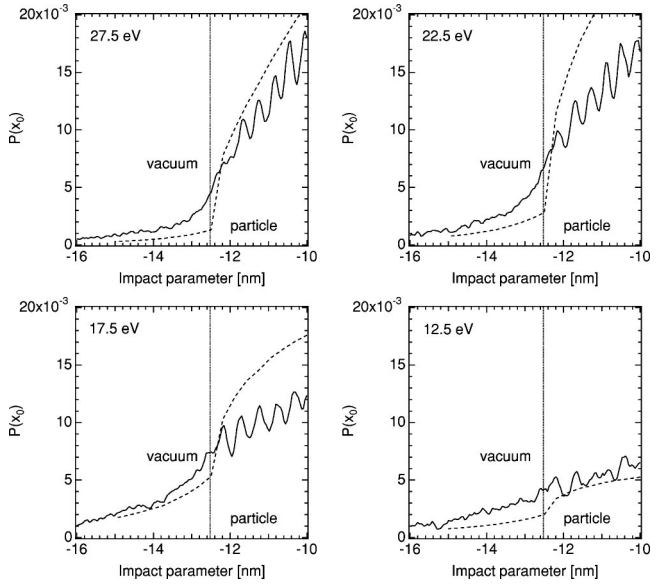

FIG. 3. Details of the interface sphere vacuum (at 12.6 nm) of the intensity line profiles shown in Fig. 2. It can be seen that the intensity does not drop to zero immediately which is a clear sign of the presence of surface excitations.

plained by the excitation of surface plasmons since volume plasmons cannot be excited when the probe electrons pass outside the particle. Figure 3 shows that our model reproduces very well the experimental data just outside the particle. At the surface plasmon resonance energy of 17 eV the simulated curve is nearly identical to the observed behavior.

The small periodic oscillations in the profiles shown in Figs. 2 and 3 are an artifact arising from the division of the raw image by the zero-loss image. The zero-loss image contains phase contrast fringes (atomic planes) resulting in a modulation of the intensity with a period determined by the interlayer distance of the graphitic shells (atomic resolution). The division operation propagates these modulations into the maps of the excitation probabilities. Images formed of inelastically scattered electrons may also show phase contrast[45,46] and we have observed it in the case of carbon nanostructures (see Ref. 41). The contrast is however much weaker than the diffraction contrast in the zero-loss filtered image and does not result in any visible effects in the image of the excitation probability or in the corresponding intensity profiles.

The minimum width of the energy window (4 eV) is imposed by the chromatic aberrations of the energy analyzer. In order to study the energy dependence of the plasmon excitation probability in more detail, we have acquired spectra of a sphere of approximately the same radius (9.7 nm) as the one analyzed in Figs. 1 to 3 at various impact parameters [Fig. 4(a)]. The spectra are compared with the simulated excitation probabilities of a sphere of 10 nm radius as shown in Fig. 4(b). The most prominent feature of the spectra is the broad peak at 27 eV when the electrons pass through the center of the sphere. Its resonance energy clearly changes as the electron probe is moved towards the sphere boundary. This behavior can be explained by the dielectric response theory, which correctly reproduces the energy shift from 27 to 17 eV [Fig. 4(b)] (for more details about the simulations, see Ref. 39). Using the results of the simulations, we can say that the

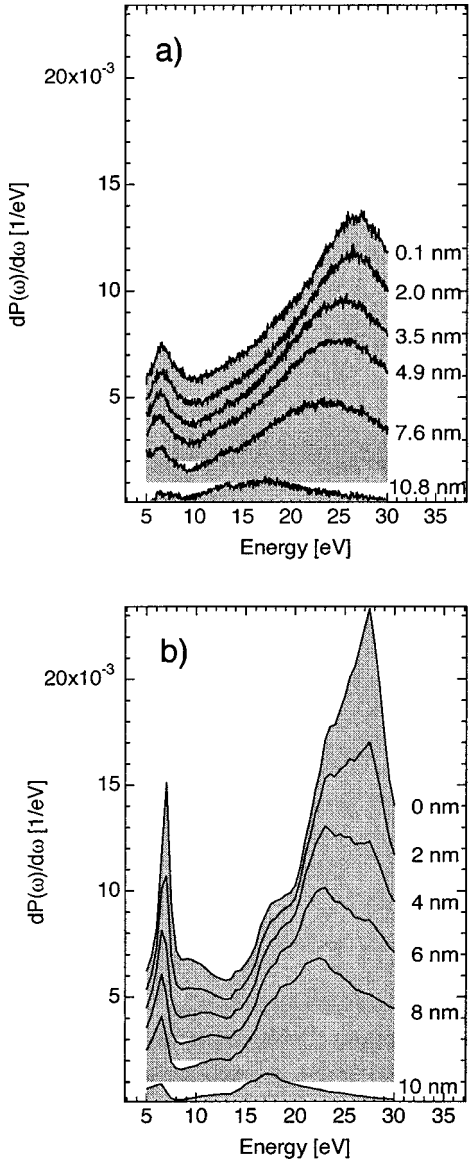

FIG. 4. (a) Electron energy-loss spectra of a multi-wall fullerene of 9.7 nm diameter compared to (b) simulated spectra for an anisotropic sphere of approximately the same size (10 nm). The different curves represent spectra taken at different impact parameters: top curves are obtained in the center of the sphere and bottom curves just outside the sphere.

shift is principally due to the continuous change in orientation of the graphitic layers as the impact parameter is increased from zero to the sphere radius. When the electron passes through the center of the sphere, it crosses graphitic layers oriented with the *c* axis parallel to the electron trajectory. Therefore, the spectrum is essentially identical to that of planar graphite of the same thickness oriented accordingly and the peak at 27 eV can be assigned to the collective resonance of the $\sigma+\pi$ electrons. When the electron passes still inside the sphere but close to the boundary, the *c* axis of the graphitic layers is oriented perpendicular to the trajectory and the spectrum is very similar to the one of planar graphite with the *c* axis perpendicular to the optical axis of the TEM. The spectrum at this moment presents a rather large peak at 19 eV, which is due to the excitation of interband transitions involving the three σ electrons per carbon atom.[47]

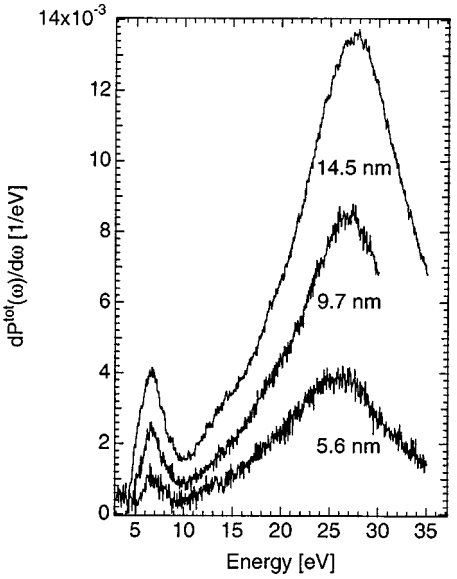

FIG. 5. Spectra acquired at zero impact parameter for three different size multiwall fullerenes: $r=14.5$ nm, $r=9.7$ nm, and $r=5.6$ nm.

The area selected spectra shown in Fig. 4 confirm the presence of surface excitations. As it was the case for the intensity line profiles (Fig. 2) surface effects can be observed best when electrons that have passed just outside the particle are analyzed. From the spectrum taken at an impact parameter of 10.8 nm [Fig. 4(a), bottom curve] the surface plasmon resonance energy of this nested concentric-shell fullerene is found to be 17 eV, exactly the value predicted by the dielectric theory model of anisotropic spheres [Fig. 4(b), bottom curve]. The effect of the presence of surface excitations is not only an additional peak in the spectrum, but also a reduction of the intensity of the volume excitation. As the impact parameter is increased from zero to the radius of the sphere, the surface contribution steadily increases and, when the electron passes outside the particle, only the surface resonance can be observed. At the same time the volume contribution is corrected to lower values (Begrenzungseffect[43]). Experimentally this is not directly visible, but the effect reinforces the shift of the electron plasmon peak from 27 to 17 eV as the probe is moved from the sphere center towards the boundary of the particle (see Refs. 39 or 41 for more details).

The other dominant feature in the loss spectrum of multiwall fullerenes is the peak at 6.5 eV. The spectrum taken close to the center of the sphere can be compared to the excitation probability of planar graphite with the *c* axis parallel to the optical axis so that the peak can be attributed to the collective resonance of the π electrons. As the probe is moved closer to the sphere boundary the resonance energy of this peak is also shifted to lower values. The reason for this shift is again the change in orientation of the graphitic layers and the presence of surface effects.

B. Size dependence and particular features

Figure 5 shows the spectra of three different size multiwall fullerenes acquired at zero impact parameter. This size range is representative of the multiwall fullerenes that were accessible experimentally. Smaller particles could not be investigated because of the limits of the experimental method: their response is hidden in the surface excitations of the support (see Ref. 41 for more details). On the other hand, larger concentric-shell fullerenes could not be produced since a more intense electron beam would have been necessary.

Figure 5 shows that in the investigated size range all spectra have the same shape. The only visible difference is the scaling of the excitation probability proportional to the size of the particles. This is somewhat surprising. One would expect the effects of the curvature of the graphitic shells to become gradually stronger as the particle size is decreased. In the case of larger multiwall fullerenes the contribution of the the outer and hence flatter layers to the EELS signal can expected to be similar to the response of planar graphite. As the diameter decreases, the influence of the high curvature of the innermost shells should become observable. Our measurements clearly show that for the investigated size range no such size dependence is detected.

We have analyzed in detail the peak position as a function of the impact parameter for the three sizes of multiwall fullerenes discussed in Fig. 5. The resonance energies have been determined from area selected spectra of the multiwall fullerenes after removal of the zero-loss peak. The results are shown in Fig. 6.

Comparing the experimental values of the resonance energy of the $\sigma+\pi$ plasmon peak (squares) as a function of the impact parameter with the theoretical curve (line with squares) it can be observed that the experimental energy shift occurs more gradually than it could be expected from the simulations. This tendency can be observed throughout the investigated size range. The difference between the experimental and simulated values is probably principally due to the fact that the electrons are not collected from an infinitely small area. The electrons entering the spectrometer come from a finite area of approximately 1.5 nm in diameter. In consequence the rather abrupt transition which is predicted at an impact parameter of about one third of the particle radius is smeared out over a larger distance. Comparing the $\sigma+\pi$ plasmon resonance energy close to the center of different size particles it can be noticed that the resonance is shifted to lower energies as the spheres become smaller. This is in contradiction to what is observed in the case of small metallic particles[48–50] where the volume plasmon resonance energy has tendency to rise to higher values. In the case of metallic particles, this blueshift is ascribed to the effect of dispersion in a finite medium. A detailed theoretical analysis of the problem based on hydrodynamic theory[51] confirms this interpretation and shows that such effects are likely to occur for spheres of radii smaller than 4 nm. It is therefore likely that the behavior we observe for multiwall fullerenes is due to the size of the analyzed portion of the sphere rather than to dispersion effects. The zone that is analyzed has a diameter of 1.5 nm. If the nested concentric-shell fullerene is small and if the center is not precisely placed over the spectrometer entrance aperture, the zone where the resonance energy is expected to drop to lower values contributes to the signal that is analyzed. This might be sufficient to make the resonance frequency in the center of the sphere appear to be lower than the actual value.

Concerning the comparison between the simulated and experimental values of the π plasmon resonance it can be

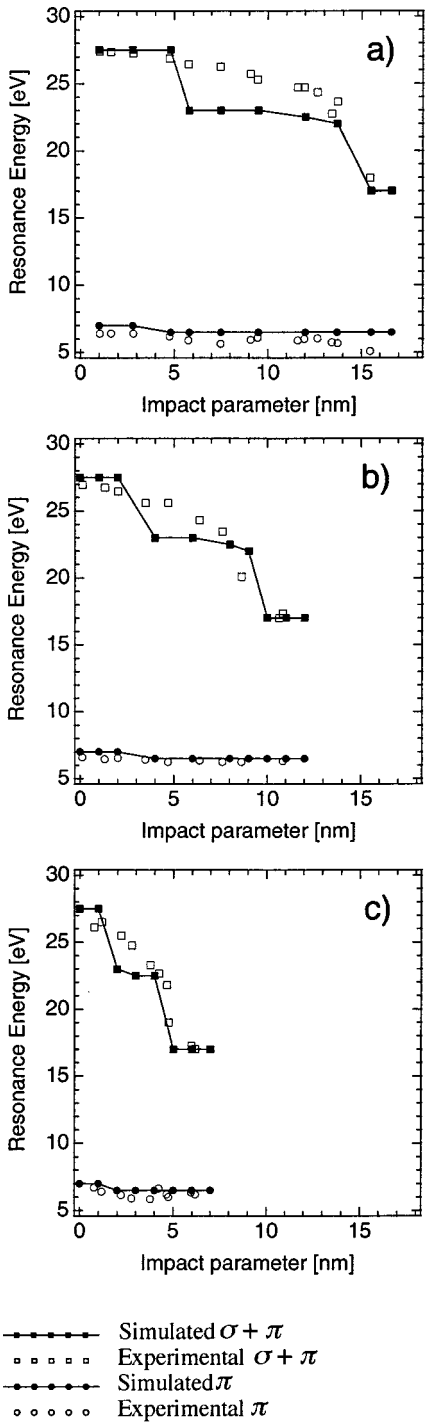

FIG. 6. Evolution of the π (circles) and the $\sigma+\pi$ (squares) plasmon peak position as a function of the impact parameter for three different sizes of particles: (a) 15 nm, (b) 10 nm and (c) 5 nm. The continuous lines represent the values obtained from the simulations.

said that the measured values are systematically lower for all impact parameters than those predicted by dielectric theory. In the frame of a free electron model the resonance frequency is given by the relation

$$\omega_p^2=\frac{ne^2}{\epsilon_0 m_e} \tag{10}$$

so that a lower resonance energy can result from either a reduced number of electrons participating in the oscillation or from a higher effective electron mass. Both of these changes would result from a modified electronic structure due to the curvature of the graphitic layers. One might expect this effect to be more pronounced in the center of the sphere, but the impact parameter dependence of the resonance frequency is well reproduced by our model (Fig. 6). This means that even if the electron is passing through the center of the sphere the energy loss in the outer (less curved) layers dominates the signal and what we observe is a constant (mean) shift of the resonance frequency at any impact parameter.

C. Differences between the experimental data and the simulations

The comparison of the simulations with the experimental data reveals that the behavior of the most prominent features of the spectra as well as the shape of the intensity line profiles at different loss energies are correctly reproduced by the model. Most of the observed tendencies of the experimental data can therefore be interpreted. However, the experimental data differ from the simulations in a few aspects.

Most important, the simulations systematically overestimate the excitation probability. As pointed out, the simulations have been carried out for ideal experimental conditions. It can be expected that the experimental peaks are broader and at the same time less intense than the simulated probabilities.[52] However, the non-interacting electron beam has a full width at half maximum of only 0.5 eV in the case of the Hitachi HF 2000 microscope and of 0.9 eV in the Philips CM 300 microscope. This small energy spread can by no means explain the observed differences. A possible explanation for this might be found in the theoretical work by Yannouleas *et al.*[53,54] Their results suggest that the excitation of the $\sigma+\pi$ and the π electron plasmons are heavily damped in the case of nested concentric-shell fullerenes. This is attributed to the fact that due to curvature, the coupling between the electrons on the spherical shells is different from the coupling in the planar case. Our experimental data might contain evidence for this phenomenon, but at present it is too early to conclude on this point. In fact, the model of the plasmon excitations of multishell fullerenes is based on three main assumptions. First, the theory has been developed in the nonrelativistic approximation. Garcia-Molina *et al.* have shown that the excitation probabilities simulated within this restriction are typically lower than those obtained when relativistic effects are considered.[55] The effect is more pronounced when the real part of the dielectric function is large and depends on the impact parameter of the incident electron. Second, the model does not take into account diffraction effects. The probe electrons do not move through the particle on a straight line as assumed in our model. Diffraction causes the electrons to deviate from the assumed trajectory and, in consequence, the investigated area is larger than initially assumed. Diffraction effects mainly affect the volume plasmon and are more pronounced in thicker regions of the sample. Some of the differences between the experimental data and the simulations could be due to this two phenomena. The third assumption that has been made is the neglect of quasielastic scattering due to the excitation of phonons. In the case of thin specimen such as

the investigated carbon particles, this should not lead to any significant errors in the simulated excitation probabilities. A possibility to determine if the observed differences are a consequence of plasmon damping or whether they are due to the assumptions made in our calculations might be a comparative study between the plasmon-loss EEL data of spherical and tubular structures. In their study Yannouleas *et al.* have also analyzed the case of carbon nanotubes.[53,54] The comparison between the expected behavior of spherical and tubular structures suggests that the plasmons in the tube case should be damped to a lesser extent. An comparative study of the experimentally determined plasmon excitation probability of multiwall fullerenes and multiwall carbon nanotubes based on nonrelativistic local dielectric response theory of spherical[39] and cylindrical[56] anisotropic particles could give valuable information about this point. However, even though EEL spectra of individual carbon nanotubes have already been published, a direct comparison with our data on spheres is not possible at the moment since the plasmon excitation probability has not been derived from the raw data.

Another difference between the experimental data and the simulations can be found in the energy range between 8 and 15 eV. The model predicts a small feature at around 10 eV and a local minimum of the excitation probability at 14 eV. Comparing with the experimental data, this cannot be observed: the minimum is at 10 eV and from there the $\sigma+\pi$ plasmon peak starts to rise. Moreover, a small local maximum can be observed at 14 eV when the electron passes close to the sphere boundary. It has been outlined in Ref. 39 that in the energy range in question the controversy about the dielectric tensor of graphite results in minor differences in the simulations if EELS or optical data is used as input for the numerical evaluation. However, neither data set can reproduce the experimental data. In consequence, we attribute the difference between the simulations and the experimental data in this energy range to a change of the electronic properties of graphite resulting from the curvature of the sheets.

IV. CONCLUSION

The comparison of the experimental data of nested concentric-shell fullerenes with the simulations carried out in the frame of the nonrelativistic local dielectric response of anisotropic spheres has allowed us to gain a detailed understanding of the plasmon excitations of these particles. The origin of the prominent features of the spectra, the variations of the resonance energies as a function of the impact parameter as well as the evolution of the intensity line profiles across the energy filtered images for different energy windows could thus be explained.

Interestingly, we observe several differences between the model and the simulations. In particular, the simulations overestimate the excitation probabilities of both the $\sigma+\pi$ and the π electron volume plasmons. This might be attributed to the damping of the plasmons which was predicted from theoretical considerations for spherical carbon nanostructures. At present this interpretation is still speculative. However, the comparison of the plasmon losses of carbon nanotubes with those of the multiwall fullerenes based on our models might give further evidence for this in the future. We suggest that the remaining differences in the energy range between 10 and 15 eV arise from intrinsic changes of the electronic properties of nested concentric-shell fullerenes due to the curvature of the graphitic shells.

For the sizes of particles that were experimentally accessible we have not been able to determine any major size-dependent variations of the electronic properties. They all seem to be in the size range where the electromagnetic properties are still determined by the bulk properties of the material. The observed differences are mainly due to the presence of a limiting surface and not to the intrinsic changes in the properties of the material (quantal size effects).

ACKNOWLEDGMENTS

The authors are grateful to D. Ugarte, L. Forró, and J.-P. Salvetat for many helpful discussions on the subject of EELS and multishell fullerenes. The experiments have been realized with the help of M. Fazan and the technical staff of the electron microscopy center in Lausanne. Their support is gratefully acknowledged. This work was partially financed by the Swiss National Science Foundation, Grant No. 2100-037660.

*Electronic address: thomas.stoeckli@epfl.ch

[1] D. Ugarte, Nature (London) **359**, 707 (1992).
[2] F. Banhart, T. Füller, Ph. Redlich, and P.M. Ajayan, Chem. Phys. Lett. **269**, 349 (1997).
[3] H.W. Kroto, J.R. Health, S.C. O'Brian, R.F. Curl, and R.E. Smalley, Nature (London) **381**, 162 (1985).
[4] By definition, all fullerenes are composed of a single graphene layer. Throughout this text, the term ''single-wall fullerene'' is used in order to clearly make the difference between the multiwall fullerenes (''carbon onions'') and C_{60}-like structures.
[5] S. Iijima and T. Ichihashi, Nature (London) **363**, 603 (1993).
[6] D.S. Bethune, C.H. Kiang, M.S. de Vries, G. Gorman, R. Savoy, J. Vazquez, and R. Beyers, Nature (London) **363**, 605 (1993).
[7] S. Iijima, Nature (London) **354**, 56 (1991).
[8] S.H. Yang, C.L. Pettiette, J. Conceicao, O. Cheshnovsky, and R.E. Smalley, Chem. Phys. Lett. **139**, 233 (1987).
[9] W. Krätschmer, L.D. Lamb, K. Fostiropoulos, and D.R. Huffman, Nature (London) **347**, 354 (1990).
[10] A. Skumanich, Chem. Phys. Lett. **182**, 486 (1991).
[11] P.L. Hansen, P.J. Fallon, and W. Krätschmer, Chem. Phys. Lett. **181**, 367 (1991).
[12] A.F. Hebard, M.J. Rosseinsky, R.C. Haddon, D.W. Murphy, S.H. Glarum, T.T.M. Palastra, A.P. Ramirez, and A.R. Kortan, Nature (London) **350**, 600 (1991).
[13] N. Hamada, S. Sawada, and A. Oshiyama, Phys. Rev. Lett. **68**, 1579 (1992).
[14] J.W. Mintmire, B.I. Dunlap, and C.T. White, Phys. Rev. Lett. **68**, 631 (1992).
[15] R. Saito, G. Fujita, G. Dresselhaus, and M.S. Dresselhaus, Appl. Phys. Lett. **60**, 2204 (1992).
[16] X.B. Zhang, X.F. Zhang, D. Bernaerts, G. Van Tandeloo, S. Amelinckx, J. Van Landuyt, V. Ivanov, J.B. Nagy, Ph. Lambin,

and A.A. Lucas, Europhys. Lett. **27**, 141 (1994).
[17] K. Akagi, R. Tamura, M. Tsukada, S. Itoh, and S. Ihara, Phys. Rev. Lett. **74**, 2307 (1995).
[18] J.P. Lu, Phys. Rev. Lett. **74**, 1123 (1995).
[19] P.J. Lin-Chung and A.K. Rajagopal, Phys. Rev. B **49**, 8454 (1994).
[20] B.I. Yakobson, C.J. Brabec, and J. Bernholc, Phys. Rev. Lett. **76**, 2511 (1995).
[21] T.W. Ebbesen and P.M. Ajayan, Nature (London) **358**, 220 (1992).
[22] A. Thess, R. Lee, P. Nikolaev, H. Dai, P. Petit, J. Robert, Ch. Xu, Y.H. Lee, S.G. Kim, D.T. Colbert, G. Scuseria, T. Tomanek, J.E. Fischer, and R.E. Smalley, Science **273**, 483 (1996).
[23] C. Journet, W.K. Maser, P. Bernier, A. Loiseau, M. Lamy de la Chapelle, S. Lefrant, P. Deniard, R. Lee, and J.E. Fischer, Nature (London) **388**, 756 (1997).
[24] J.-M. Bonard, T. Stora, J.-P. Salvetat, F. Maier, T. Stöckli, K. Duschl, L. Forró, W. de Heer, and A. Châtelain, Adv. Mater. **9**, 827 (1997).
[25] E. Dujardin, T.W. Ebbesen, A. Krishnan, and M.M.J. Treacy, Adv. Mater. **10**, 611 (1998).
[26] J.-M. Bonard, T. Stöckli, W. A. de Heer, A. Châtelain, J.-C. Charlier, X. Blase, A. De Vita, R. Car, J.-P. Salvetat, and L. Forró (unpublished).
[27] J.-P. Salvetat, A. J. Kulik, G. A. D. Briggs, J.-M. Bonard, T. Stöckli, N. Burnham, and L. Forró, Adv. Mater. **11**, 161 (1999).
[28] R.W. Odom, J.-L. Huang, P. Kim, and C.M. Lieber, Nature (London) **391**, 62 (1998).
[29] J.W.G. Wildöer, L.C. Venema, A.G. Rinzler, R.E. Smalley, and D. Dekker, Nature (London) **391**, 59 (1998).
[30] S.J. Tans, M.H. Devoret, R.J.A. Groeneveld, and C. Dekker, Nature (London) **394**, 761 (1998).
[31] A. Bachtold, M. Henry, C. Terrier, C. Strunk, C. Schönenberger, J.-P. Salvetat, J.-M. Bonard, and L. Forró, Appl. Phys. Lett. **73**, 274 (1998).
[32] T. Cabioc'h, J.C. Girard, M. Jaouen, M.F. Denanot, and G. Hug, Europhys. Lett. **38**, 471 (1997).
[33] P. Wesolowski, Y. Lyutovich, F. Banhart, H.D. Carstanjen, and H. Kronmüller, Appl. Phys. Lett. **71**, 1948 (1997).
[34] Ph. Redlich, F. Banhart, Y. Lyutovich, and P.M. Ajayan, Carbon **36**, 561 (1998).
[35] F. Banhart and P.M. Ajayan, Nature (London) **382**, 433 (1996).
[36] Z.L. Wang, Micron **27**, 265 (1996).
[37] A.A. Lucas, L. Henrard, and Ph. Lambin, Phys. Rev. B **49**, 2888 (1994).
[38] L. Henrard, F. Malengreau, F. Rudolf, K. Hevesi, R. Caudano, Ph. Lambin, and Th. Cabioc'h, Phys. Rev. B **59**, 5832 (1999).
[39] T. Stöckli, J.-M. Bonard, A. Châtelain, Z.L. Wang, and P. Stadelmann, Phys. Rev. B **57**, 15 599 (1998).
[40] R. F. Egerton, *Electron Energy-Loss Spectroscopy in the Electron Microscope*, 2nd ed. (Plenum, New York, 1996).
[41] T. Stöckli, Ph.D. thesis, Swiss Federal Institute of Technology of Lausanne, 1999.
[42] D.L. Misell and A.F. Jones, J. Phys. A **2**, 540 (1969).
[43] H. Souchay, Ph.D. thesis, Ecole Centrale Paris, 1999.
[44] H. Boersch, J. Geiger, and W. Stickel, Z. Phys. **212**, 130 (1968).
[45] A. Howie, Proc. R. Soc. London **271**, 268 (1963).
[46] Z.L. Wang and J. Bentley, Microsc. Microanal. Microstruct. **2**, 177 (1992).
[47] E.A. Taft and H.R. Philipp, Phys. Rev. **138**, 197 (1965).
[48] M. Achèche, C. Colliex, H. Kohl, A. Nourtier, and P. Trebbia, Ultramicroscopy **20**, 99 (1986).
[49] M. Achèche, C. Colliex, and P. Trebbia, Scan Electron Microscopy **1**, 25 (1986).
[50] T. Stöckli, P. Stadelmann, and A. Châtelain, Microsc. Microanal. Microstruct. **8**, 145 (1997).
[51] Z.L. Wang and J.M. Cowley, Ultramicroscopy **23**, 97 (1987).
[52] Deconvolution of the data with the experimental zero-loss peak cannot eliminate the experimental broadening due to the energy distribution of the incident electrons.
[53] C. Yannouleas, E.N. Bogachek, and U. Landman, Phys. Rev. B **50** 7977 (1994).
[54] C. Yannouleas, E.N. Bogachek, and U. Landman, Phys. Rev. B **53**, 10 225 (1996).
[55] R. Garcia-Molina, A. Gras-Marti, A. Howie, and R.H. Ritchie, J. Phys. C **18**, 5335 (1985).
[56] T. Stöckli, J.-M. Bonard, A. Châtelain, Z. L. Wang, and P Stadelmann, Philos. Mag. B **79**, 1531 (1999).